Journal Pre-proof

A biochar catalyst with functional Brønsted–Lewis acid sites for enhancing hydroxymethylfurfural production from glucose

Kamonwat Nakason , Saran Youngjan , Vorapot Kanokkantapong , Wanwitoo Wanmolee , Wasawat Kraithong , Parinvadee Chukaew , Kriangsak Riewklang , Tokla Eom , Pongtanawat Khemthong , Bunyarit Panyapinyopol

PII: S2772-4433(25)00058-3
DOI: https://doi.org/10.1016/j.recm.2025.100148
Reference: RECM 100148

To appear in: *Resources Chemicals and Materials*

Received date: 27 July 2025
Revised date: 14 November 2025
Accepted date: 16 November 2025

Please cite this article as: Kamonwat Nakason , Saran Youngjan , Vorapot Kanokkantapong , Wanwitoo Wanmolee , Wasawat Kraithong , Parinvadee Chukaew , Kriangsak Riewklang , Tokla Eom , Pongtanawat Khemthong , Bunyarit Panyapinyopol , A biochar catalyst with functional Brønsted–Lewis acid sites for enhancing hydroxymethylfurfural production from glucose, *Resources Chemicals and Materials* (2025), doi: https://doi.org/10.1016/j.recm.2025.100148

Highlights

- Cassava rhizome (CR) biochar served as a support for Brønsted–Lewis acid catalysts.
- Analyses reveal the catalyst possesses acid functions and porous textural features.
- Biochar-based catalyst enabled HMF production from glucose in eco-friendly system.
- Maximum HMF yield (34.5%) achieved in 3:2 of isopropanol: H_2O at 200 °C for 75 min.

A biochar catalyst with functional Brønsted–Lewis acid sites for enhancing hydroxymethylfurfural production from glucose

Kamonwat Nakason[a], Saran Youngjan[b], Vorapot Kanokkantapong[c,d], Wanwitoo Wanmolee[e,f], Wasawat Kraithong[b], Parinvadee chukaew[a], Kriangsak Riewklang[a], Tokla Eom[a], Pongtanawat Khemthong[b]*, Bunyarit Panyapinyopol[a]*

[a]*Department of Sanitary Engineering, Faculty of Public Health, Mahidol University, Bangkok, Thailand*

[b]*National Nanotechnology Center (NANOTEC), National Science and Technology Development Agency (NSTDA), Pathumthani, Thailand*

[c]*Department of Environmental Science, Faculty of Science, Chulalongkorn University, Bangkok, Thailand*

[d]*Research Group (STAR): Waste Utilization and Ecological Risk Assessment, the Ratchadaphiseksomphot Endowment Fund, Chulalongkorn University, Bangkok 10330, Thailand*

[e]*Department of Chemical Engineering, Faculty of Engineering, King Mongkut's University of Technology North Bangkok (KMUTNB), Bangkok, 10800, Thailand*

[f]*Center of Eco-Materials and Cleaner Technology, King Mongkut's University of Technology North Bangkok, Bangkok 10800, Thailand*

[*]*Corresponding author:*

Tel.: +662 564 7100, Email address: pongtanawat@nanotec.or.th

Tel.: +662 354 8540, Email address: bunyarit.pan@mahidol.ac.th

Abstract

The sustainable production of 5-hydroxymethylfurfural (HMF) from glucose remains a major challenge in advancing bio-based chemical platforms. Despite extensive research, achieving high HMF yields in environmentally friendly systems is hindered by the complexity of glucose conversion pathways. This study presents a novel bifunctional catalyst (B-TsFe), derived from cassava rhizome (CR) biochar and functionalized with Brønsted and Lewis acid sites. The catalyst design leverages the carbon-rich nature of CR, integrating *p*-toluenesulfonic acid (TsOH) and ferric chloride ($FeCl_3$) to establish synergistic acid functionalities. Comprehensive characterization confirmed the presence of both acid site types and mesoporous structures conducive to catalytic activity. The catalyst's performance was evaluated in a water–isopropanol (iPrOH) biphasic system, achieving a maximum HMF yield of 34.5 wt.% under optimized conditions (200 °C, 75 min, 3:2 iPrOH:H_2O ratio). Furthermore, the catalyst maintained high activity over five reuse cycles with minimal loss in performance. Compared to conventional biochar-based catalysts, B-TsFe exhibits superior acidity, enhanced glucose conversion efficiency, and a lower environmental impact due to its renewable origin and green solvent system. This work offers an eco-efficient strategy for HMF synthesis, addressing key limitations in catalyst development and process sustainability.

Keywords: 5-hydroxymethylfurfural, intermediate chemical, cassava rhizome, heterogeneous catalyst, biofuel

1. Introduction

The growing depletion of fossil resources has intensified global efforts to transition toward a bioeconomy that leverages renewable feedstocks for the sustainable production of biofuels and high-value chemicals. Among promising platform chemicals, 5-hydroxymethylfurfural (HMF) has emerged as a versatile intermediate for bio-based polymers, fuels, pharmaceuticals, and other industrial applications [1]. Its synthesis from carbohydrates, particularly glucose, offers a sustainable route to produce valuable chemicals such as 2,5-furandicarboxylic acid (FDCA), 2,5-diformyfuran (DFF), 2,5-dimethylfuran (2,5-DMF), and 2,5-bis(hydroxymethyl)furan [2-5]. However, HMF production from glucose involves complex reaction steps, including isomerization and dehydration, typically catalyzed by Lewis acids (glucose-to-fructose isomerization) [6] and Brønsted acids (fructose dehydration) [7]. Developing an efficient Brønsted–Lewis hybrid acid catalyst that integrates both functionalities remains a key challenge [8-12].

Recent research has focused on heterogeneous catalysts for HMF production from glucose [13-18]. Biochar-based catalysts, in particular, offer notable advantages due to their renewable origin, low carbon footprint, and tunability [18-20], unlike conventional catalysts such as zeolites, MOFs, resins, and silica, which generally have positive carbon footprints [21-24]. Notably, hybrid acid catalysts derived from oil palm empty fruit bunches (POFB) and birch sawdust, using sulfuric acid (H_2SO_4) as a Brønsted acid source, have shown promise in HMF production [25, 26]. However, due to the corrosive nature and recyclability limitations of H_2SO_4, *p*-toluenesulfonic acid (TsOH) has gained attention as a milder and more environmentally friendly alternative [18, 27]. Cassava rhizome (CR), a major agricultural byproduct in Thailand, connects the root and stalk of the cassava plant and is often disposed of by open-field burning, contributing to air pollution [11]. CR contains abundant carbon, oxygen, sulfur, and inorganic elements, which, upon pyrolysis, give rise to biochar rich in oxygen- and sulfur-containing functional groups [11, 28]. The oxygen-containing groups (e.g., carboxyl,

hydroxyl) can act as weak acid sites, while sulfur groups can form strong –SO_3H functionalities [29]. Despite its potential, CR-derived biochar-based Brønsted–Lewis acid catalysts prepared using TsOH have not yet been explored.

In addition to catalyst design, solvent systems critically influence HMF yield and selectivity. Prior studies employed complex biphasic systems such as N-methyl-2-pyrrolidone (NMP)–H_2O/MIBK with NaCl [25], or H_2O/THF mixtures [26]. However, these systems require large volumes of immiscible organic solvents and rely on fossil-derived components, complicating extraction and reducing sustainability [30]. To address these issues, isopropanol (iPrOH) has emerged as a green, low-boiling-point solvent (82.2°C) with excellent sugar solubility and recovery efficiency [31, 32]. Moreover, iPrOH can be derived from biomass glucose via fermentation, further enhancing process sustainability [33]. Nevertheless, HMF production from glucose using CR-derived biochar-based Brønsted–Lewis catalysts in iPrOH–H_2O systems has not been reported.

Thus, this study aimed to (1) synthesize a Brønsted–Lewis hybrid acid catalyst (B-TsFe) using CR-derived biochar functionalized with TsOH (Brønsted source) and $FeCl_3$ (Lewis source), (2) evaluate its performance for HMF production from glucose in an iPrOH:H_2O biphasic system, and (3) investigate the effects of reaction temperature, reaction time, and solvent ratio on HMF yield and selectivity.

2. Material and methods

2.1. Catalyst synthesis and characterization

Cassava rhizome (CR), sourced from Phetchabun province, Thailand, was processed using a hammer mill to obtain a powder with a particle size range of 300–600 μm [28, 34, 35]. The sieved powder was stored in airtight plastic bags for subsequent use. The bifunctional Brønsted–Lewis acid catalyst was synthesized via two consecutive steps, including biochar

preparation and acid functionalization. In biochar preparation step, 3 g of CR powder was placed in a quartz boat and inserted into a horizontal tube furnace. The system was purged with CO_2 at 100 mL/min for 15 min to remove residual air. The sample was then heated at 700 °C and for 60 min under a continuous CO_2 flow. The resulting biochar was labeled as "B-CR".

For acid functionalization step, 1 g of B-CR was mixed with either *p*-toluenesulfonic acid monohydrate ($TsOH{\cdot}H_2O$, Sigma-Aldrich, Canada) or ferric chloride hexahydrate ($FeCl_3{\cdot}H_2O$, Qrec Co. Ltd., New Zealand) at a 1:1 mass ratio (biochar: acid precursor) [26]. The mixture was transferred to a 100 mL Teflon-lined stainless-steel autoclave (NK Laboratory Co., Ltd., Thailand), sealed, and heated at 200 °C for 6 h. After cooling rapidly in an ice bath (4–6 °C), the solid product was washed with deionized water until the pH stabilized between 5 and 6. The final solids were dried at 105 °C and stored in sealed glass vials. The synthesized catalysts were labeled as B-Ts (Brønsted), B-Fe (Lewis), and B-TsFe (hybrid). All experiments were conducted in triplicate (n = 3) to ensure reproducibility.

The B-CR and all synthesized catalysts were characterized by elemental analysis, acid-base neutralization back titration, temperature-programmed desorption (TPD), thermogravimetric analyzer (TGA), X-ray diffractometer (XRD), Raman spectroscopy, scanning electron microscopy-energy dispersive X-ray spectroscopy (SEM-EDS), transmission electron microscopy (TEM), N_2 adsorption- desorption, fourier transform infrared spectroscopy (FTIR), and X-ray photoelectron spectroscopy (XPS). Elemental composition (C, H, N, S) was determined using a CHNS analyzer (LECO CHNS628, USA). Ash content was measured following the NREL/TP-510-42622 protocol, and oxygen content was calculated by difference [36]. Total acidity and sulfonic acid group density were quantified via acid–base back titration [37]. TPD analysis was conducted using AutoChem II 2920 (Micromeritics, USA) [38]. Thermal degradation behaviors were evaluated using TGA ((NETZSCH STA 449 F5 Jupiter, Germany)) at 50 to 850 °C with a 10 °C/min heating rate under 50 mL/min N_2 gas.

Structure characteristics were explored by an XRD (Bruker D8 ADVANCE) with Cu Kα radiation; and Raman spectroscopy (High Resolution Raman, LabRAM HR Evolution) with a laser wavelength of 532 nm. Surface characteristic and elemental content were observed using SEM-EDS (Quanta 250, Czech Republic). Structural characteristics were explored using a TEM (Talos F 200X G2, Thermo Scientific, USA). Textural properties were quantified with 3Flex (Micromeritics, USA). Each sample was pretreated for 10 h at 200 °C prior measurement. The specific surface area and pore properties were further determined by the Brunauer-Emmett-Teller (BET) method and the Barrett-Joyner-Halenda (BJH) method. The functional groups of all samples were observed using a FTIR (Thermo Scientific Nicolet 6700, Thermo Scientific, USA) through the potassium bromide (KBr) pellet method in transmission mode. Prior to analysis, each sample was dried for 24 h at 105 °C. Surface chemical states were determined using XPS (Kratos Axis Ultra, Kratos, UK). The lignocellulosic and volatile matter (VM) contents of the pristine CR were measured via the method of NREL/TP-510-42618 [39] and ASTM D7582 [40], respectively. The fixed carbon (FC) content was determined by subtracting the sum of ash and VM contents from 100 %.

2.2. Synthesis and analysis of 5-hydroxymethylfurfural

In a typical batch experiment, 0.5 g of D(+)-glucose (Sigma-Aldrich, Canada), 0.05 g of catalyst, and 0.05 g of NaCl (Qrec Co. Ltd., New Zealand) were added to a Teflon-lined stainless-steel autoclave. A solvent mixture of isopropanol (iPrOH, Qrec Co. Ltd., New Zealand) and water (total volume: 20 mL) was introduced at varying volume ratios of 4:1, 3:2, and 2:3 (iPrOH:H_2O). The reactor was then sealed and heated at 160 – 200 °C for 15 – 75 min. Following the reaction, the vessel was immediately quenched in cold water (4 °C) to halt further conversion. The liquid product was separated by vacuum filtration, collected in a vial, and stored at 4 °C for subsequent analysis. The spent was washed, dried at 105 °C for 24 h, weighed, and stored in amber vials for potential reuse. All experiments were conducted

in duplicate, and average values were reported. In cases where the coefficient of variation (CV) exceeded 5%, a third replicate was performed to validate the results.

The liquid products were analyzed using high-performance liquid chromatography (HPLC) and gas chromatography–mass spectrometry (GC–MS). The concentrations of glucose and HMF were quantified by HPLC (Shimadzu 10A, Shimadzu, Japan), while additional organic species were identified by GC–MS (GC 7890A-MS 5975C, Agilent Technologies, USA). Instrumental parameters and operating conditions followed previously reported methods [11, 35, 41].

Yield and selectivity of HMF, and glucose conversion were determined using Equations (1) – (3):

$$Y = (Mp / Mi) \times 100\% \quad (1)$$

$$C = (Mc / Mi) \times 100\% \quad (2)$$

$$S = (Y / C) \times 100\% \quad (3)$$

where, Y, C, S, Mp, Mi, and Mc represent HMF yield (wt.%), glucose conversion (wt.%), HMF selectivity (%), HMF mass, initial glucose mass, and consumed glucose mass, respectively.

3. Results and discussion

3.1. CR intrinsic properties

Table 1 Compositions of intrinsic CR

Compositions		Contents
Ultimate analysis (wt.%)	C	43.7
	H	5.9
	N	1.3
	S	0.1
	O	43.9
Proximate analysis (wt.%)	Ash	5.1
	VM	75.4
	FC	19.5
Lignocellulosic compositions (wt.%)	Cellulose	36.1
	Hemicellulose	32.0
	Lignin	30.9

The intrinsic composition of cassava rhizome (CR) is summarized in Table 1. Ultimate and proximate analyses reveal that CR possesses notably higher oxygen and volatile matter (VM) contents compared to carbon and fixed carbon (FC). Moreover, lignocellulosic analysis indicates that CR is primarily composed of cellulose and hemicellulose, with comparatively lower lignin content. These characteristics, specifically the high levels of oxygen, VM, cellulose, and hemicellulose, suggest that CR is a promising precursor for producing biochar with well-developed porous structures suitable for catalyst support, particularly through devolatilization during carbonization [42, 43]. Additionally, the elevated oxygen content and abundance of surface functional groups (e.g., –OH and –COOH), as illustrated in Fig. S1, facilitate the introduction of Brønsted acid sites via sulfonation [44]. Furthermore, the presence

of inherent inorganic elements such as potassium, calcium, and magnesium, commonly found in CR ash, may aid the formation of Lewis acid sites through coordination with electron-donating groups during thermochemical activation processes [18, 45].

3.2. Biochar and catalyst characteristics

Table 2 Elemental compositions, acidic density, and specific surface area of the B-CR, B-Ts, B-Fe, B-TsFe, and spent B-TsFe

Samples	Elemental compositions (wt.%)						Acidity (mmol/g)		SSA[a]
	Carbon	Hydrogen	Nitrogen	Sulfur	Oxygen	Ash	Total	-SO_3H	(m^2/g)
B-CR	72.0	1.7	1.4	0.1	12.7	12.2	0.1	0.0	355
B-Ts	67.5	1.7	1.3	4.2	19.8	5.3	0.8	0.3	23
B-Fe	68.2	1.2	1.4	0.0	17.4	11.8	1.5	0.0	31
B-TsFe	68.6	1.8	1.5	3.7	17.5	6.9	1.6	0.2	18
Spent B-TsFe	71.4	1.8	1.4	1.3	18.0	6.1	1.0	0.1	5

[a]*Specific surface aera*

Elemental analysis of B-CR and the functionalized catalysts (Table 2) highlights changes in carbon, sulfur, oxygen, nitrogen, and ash associated with acid grafting. B-CR shows higher carbon than the functionalized samples, likely because grafting promotes partial conversion of solid carbon to gaseous products. Oxygen remaining in B-CR, attributable to incomplete carbonization, is associated with -OH and -COOH functionalities [29]. Marked increases in sulfur and oxygen in B-Ts relative to B-CR confirm successful incorporation of sulfonic groups. By contrast, B-Fe shows lower sulfur and oxygen than B-Ts and B-TsFe, indicating a lower –SO_3H density. B-TsFe exhibits higher nitrogen than B-Ts or B-Fe, potentially beneficial for glucose isomerization to fructose [46]. Acid treatment lowers ash content relative to B-CR, consistent with inorganic removal, whereas B-Fe retains the highest ash among catalysts due to iron species, confirming Fe^{3+} grafting. In the spent B-TsFe, higher carbon and lower sulfur and ash than in the fresh sample indicate acid leaching and humin deposition during HMF production [47].

Total acidity and -SO_3H site densities (Table 2) further evidence surface functionalization. B-CR had much lower total and -SO_3H acidity than the catalysts. B-Fe exhibited higher total acidity than B-Ts, while B-Ts had the highest -SO_3H density, consistent with Lewis (Fe^{3+}) and Brønsted (-SO_3H) sites, respectively. The total acidity of B-Ts exceeded its -SO_3H density, implying contributions from oxygenated groups inherited from B-CR. B-TsFe showed the highest total acidity (1.6 mmol/g) with substantial -SO_3H density, suggesting superior bifunctional (Brønsted–Lewis) activity for glucose conversion to HMF. Both metrics decreased in spent B-TsFe, reinforcing acid-site leaching during reaction [18].

Specific surface areas from N_2 adsorption–desorption isotherms (BET) are summarized in Table 2. All samples (B-CR, B-Fe, B-Ts, B-TsFe) displayed type-IV isotherms with H3 hysteresis (IUPAC), indicative of mesoporosity (Fig. S2), in agreement with SEM. Acid functionalization reduced BET surface area relative to raw B-CR, consistent with partial pore blockage or collapse by benzenesulfonic groups and metal species [26, 29]. Spent B-TsFe shows a pronounced area loss versus fresh B-TsFe, primarily due to humin accumulation blocking internal pores and active sites [48].

The thermal degradation behaviors of B-CR, B-Ts, B-Fe, and B-TsFe were evaluated using thermogravimetric analysis (TGA) and derivative thermogravimetry (DTG), as shown in Fig. S3(a) and (b), respectively. An initial mass loss at 50 and 150 °C was attributed to the evaporation of moisture and light volatiles. Beyond this range, from 150 to 850 °C, only minimal weight loss was detected, indicating that all samples exhibited high thermal stability. B-Ts and B-TsFe lose more mass than B-Fe, indicating that TsOH grafting reduces matrix stability; B-Ts has the lowest residual mass at 850 °C. Mass losses above 350 °C are associated with degradation of oxygenated groups (hydroxyl, carboxyl) [49], while losses at 210–290 °C correspond to decomposition of grafted sulfonic groups, confirming sulfonation [50]. Within

210–290 °C, B-TsFe shows a lower mass-loss rate than B-Ts, consistent with its lower –SO_3H density (Table 2).

Fig. 1. (A) NH_3-TPD profiles and (B) FTIR spectra of B-CR, B-Ts, B-Fe, and B-TsFe

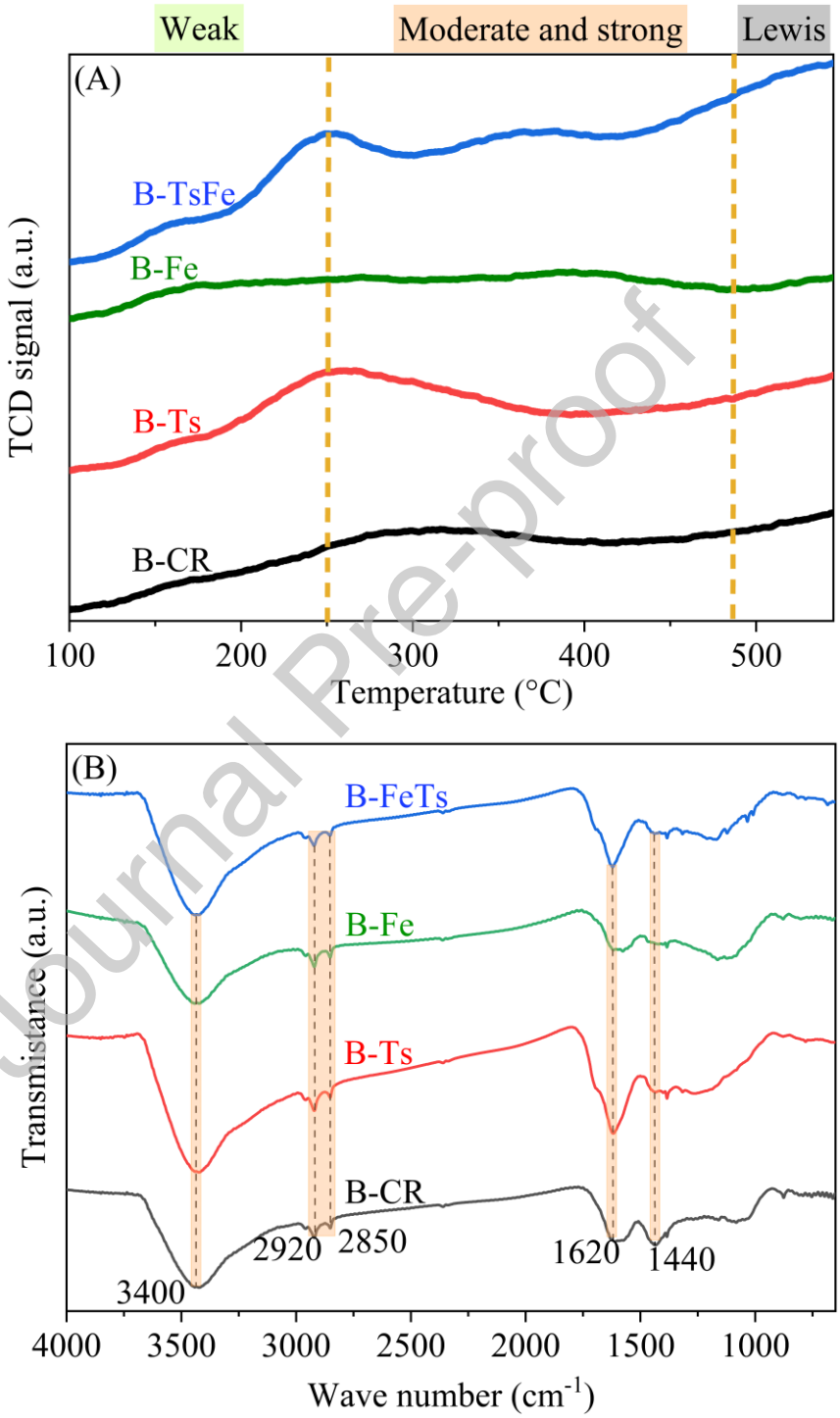

NH_3-TPD (Fig. 1(A)) shows only weak desorption for B-CR, reflecting mild acidity from oxygenated functionalities (carboxylic acids, anhydrides, lactones, lactols, and phenols)

[26]. B-Ts displays distinct peaks near 250 °C and 490 °C, indicating moderate and strong acidity [51], primarily Brønsted sites (-SO_3H) introduced by TsOH, consistent with elevated S content (Table 2) [52]. B-Fe exhibited a broad, high-temperature peak starting near 500 °C, characteristic of thermally stable Lewis sites from Fe^{3+} species [53, 54]. These results confirm the successful incorporation of acidic functionalities on the B-CR surface through acid grafting. Additionally, acid modification introduced various oxidized functionalities, such as phenolic and carboxylic acid groups, onto the B-CR surface [7, 55-57], as reflected by increased total acidity and sulfur/oxygen contents in the catalysts. The acidity of the B-Fe catalyst was slightly higher than that of raw B-CR, due to the presence of Fe_2O_3 species functioning as Lewis acid sites. Notably, the B-TsFe catalyst displayed two distinct NH_3 desorption peaks, associated with both Brønsted and Lewis acid sites, confirming its bifunctional acid nature. This dual acidity suggests a high potential for promoting both isomerization and dehydration reactions during glucose conversion to HMF.

Fourier Transform Infrared Spectroscopy (FTIR) spectra (Fig. 1(B)) revealed significant differences between B-CR and its acid-functionalized derivatives. A broad band at 3475 – 3400 cm^{-1} corresponds to O–H stretching vibrations from hydroxyl, carboxylic acid, and alcohol groups [58], with B-Ts showing the most intense signal, consistent with its high oxygen content. Peaks at 2920 and 2850 cm^{-1} represent –CH_2 asymmetric and symmetric stretching, respectively [59]. The C=O stretch of carboxylic acid groups appeared around 1720 – 1715 cm^{-1}, with the highest intensity again in the B-Ts catalyst, consistent with its acidity and elemental composition (Table 2) [60]. Aromatic C=C stretching vibrations were observed at 1598–1580 and 1620 cm^{-1} [56, 61, 62], while C–H bending appeared at 1425 cm^{-1} [38]. Further, C–O stretching, symmetric O=S=O stretching, and -SO_3H group vibrations were detected at 1230, 1162, and 1037 cm^{-1}, respectively [38, 60, 63]. The FTIR signals were generally weaker in B-CR compared to the catalysts, consistent with its lower total acidity and

-SO_3H group density. Additionally, aromatic C–H out-of-plane bending was observed in the 900–750 cm^{-1} region [59].

Fig. 2. (A) XRD patterns, and (B) Raman peaks of B-CR, B-Ts, B-Fe, and B-TsFe

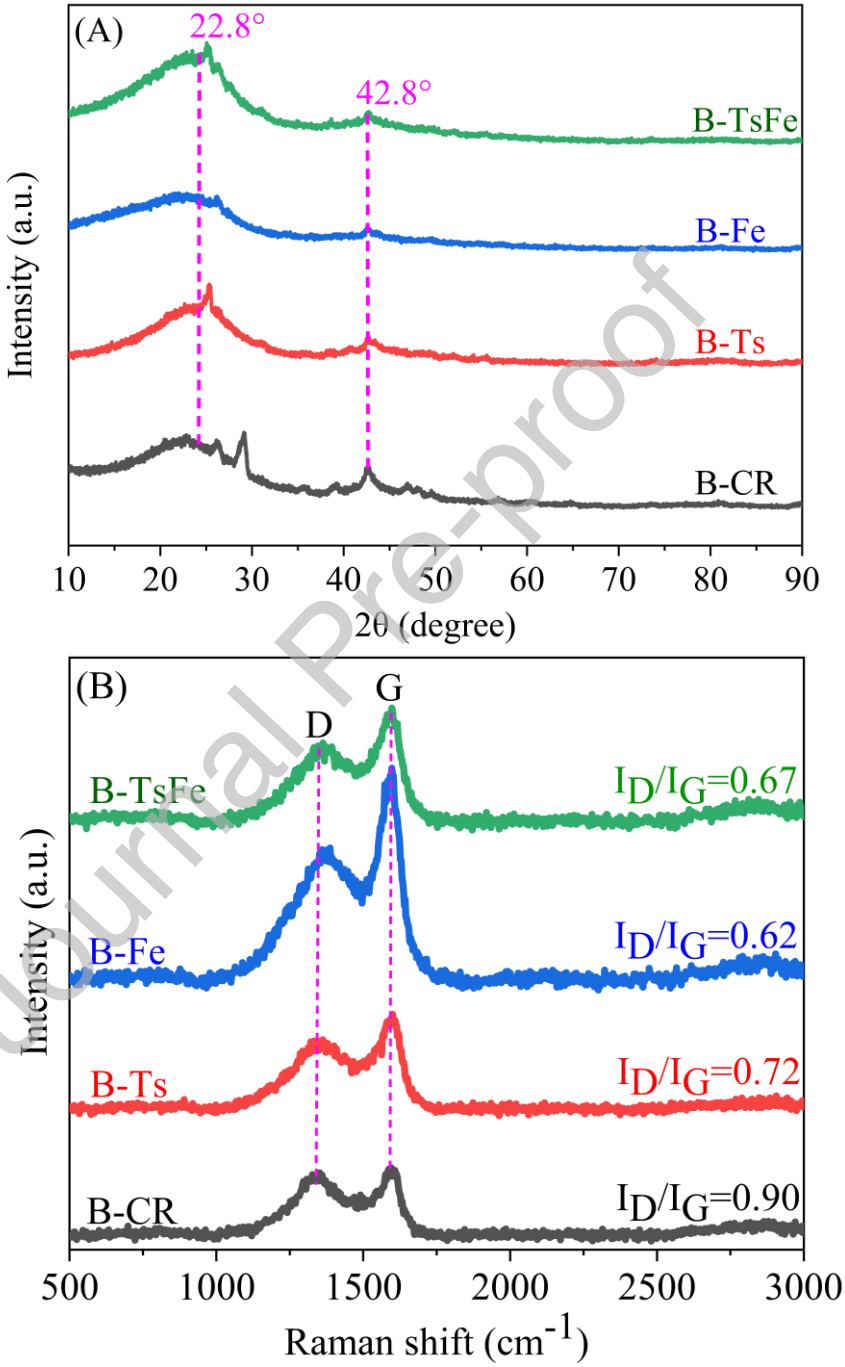

The structural properties of B-CR, B-Ts, B-Fe, and B-TsFe were analyzed using X-ray diffraction (XRD) patterns (Fig. 2(A)) and Raman spectroscopy (Fig. 2(B)). In the XRD profiles, all samples exhibited a broad diffraction peak centered around 22.8°, corresponding

to the (002) plane of turbostratic graphite, indicative of disordered aromatic carbon layers [64]. A small peak at 2θ of 43.8° was attributed to the (100) plane of graphitic carbon [65]. Notably, the intensity of these peaks decreased in B-Ts, B-Fe, and B-TsFe, suggesting a reduction in graphitization following acid functionalization. Raman spectra were employed to further evaluate the defect structures within the carbon matrix. All samples showed characteristic D and G bands at 1331 and 1595 cm^{-1}, respectively [66]. The D-band arises from the A_1g breathing mode of disordered carbon (defects), while the G-band is associated with the E_2g stretching mode of sp^2 -hybridized carbon atoms. The intensity ratio of the D to G band (I_D/I_G) is commonly used to assess the degree of disorder and defect concentration [67]. The calculated I_D/I_G ratios for B-CR, B-Ts, B-Fe, and B-TsFe were 0.90, 0.72, 0.62, and 0.67, respectively. The higher I_D/I_G value of B-CR (0.90) reflects a higher degree of structural disorder and porosity. After functionalization, this ratio decreased, indicating that the introduction of benzenesulfonic acid groups and Fe species partially passivated surface defects and obstructed some pore structures. These observations confirm the structural modification and reduced defect density resulting from acid and metal grafting processes.

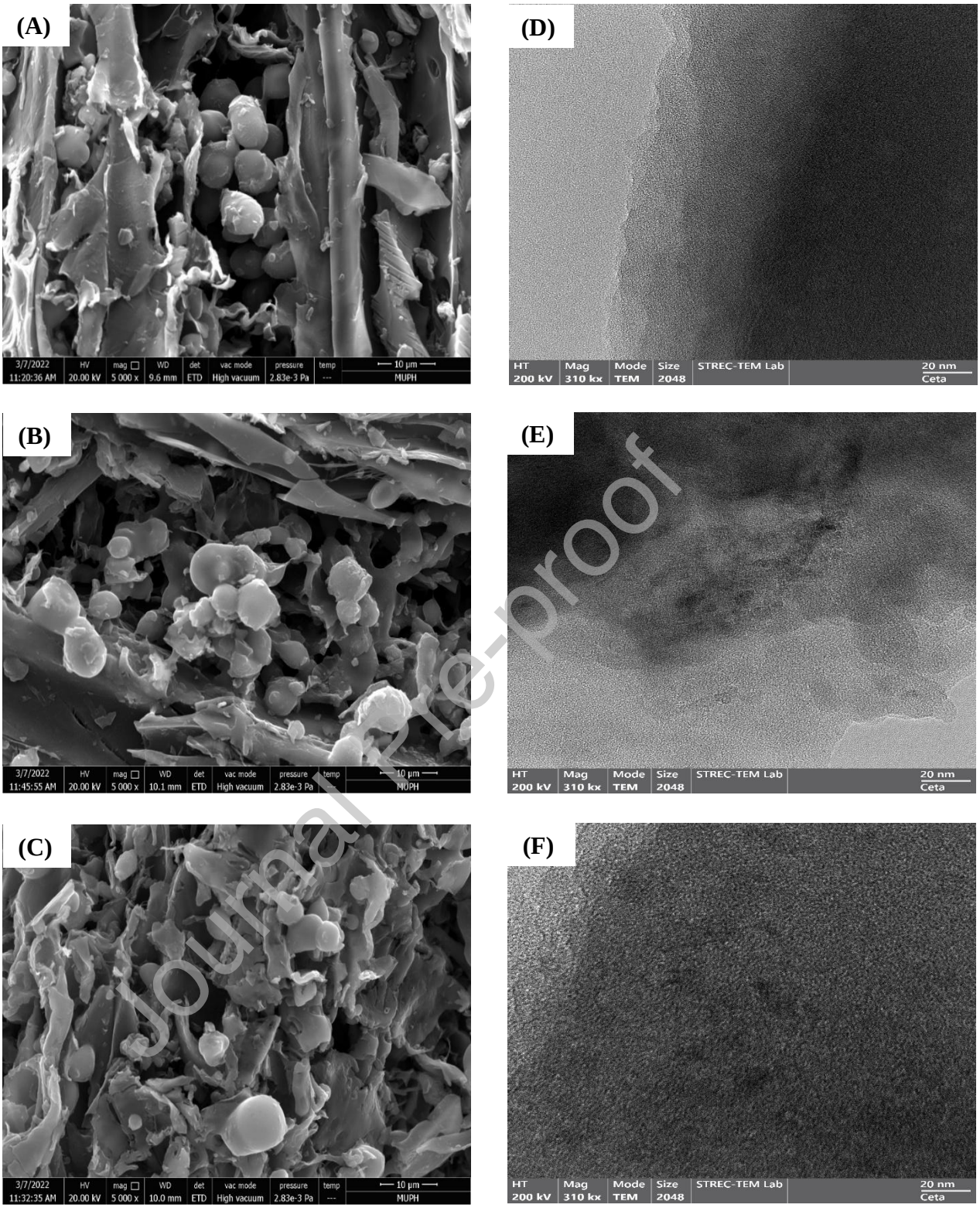

Fig. 3. SEM images of (A) B-Ts, (B) B-Fe, and (C) B-TsFe catalysts; and TEM images of (D) B-Ts, (E) B-Fe, and (F) B-TsFe catalysts

SEM (Fig. S4) shows a smooth pristine CR surface that becomes fractured and microporous after carbonization at 700 °C(B-CR), due to devolatilization and

depolymerization [68]. Acid-functionalized catalysts (Fig. 3(A)–(C)) are more disordered and porous structures compared to B-CR. Notably, the B-Fe catalyst showed a rougher surface with pronounced cracks and grooves, attributed to the stronger acidity of $FeCl_3$ compared to TsOH, which induced more aggressive surface etching. Mesopores (2–50 nm) evident on catalyst surfaces should enhance mass transfer and HMF productivity [69]. TEM analysis further supported these findings. As depicted in Fig. S5, B-CR exhibited a relatively translucent structure, while the B-Ts catalyst (Fig. 3(D)) displayed uniformly denser regions, indicating successful incorporation of benzenesulfonic acid groups into the porous framework. In the B-Fe catalyst (Fig. 3(E)), iron nanoparticles were observed within the porous, translucent biochar matrix. Meanwhile, the B-TsFe catalyst (Fig. 3(F)) showed iron nanoparticles embedded within denser regions, suggesting that the co-grafting of Fe species and benzenesulfonic acid groups partially obstructed or collapsed the original pore network, consistent with the reduced surface area and porosity observed in the BET analysis. EDS results (Fig. S6(A)–(D)) revealed that all samples predominantly composed of carbon, while the functionalized catalysts (B-Ts, B-Fe, B-TsFe) contained significantly higher oxygen and sulfur contents than B-CR. The B-TsFe catalyst also exhibited elevated levels of iron (Fe), sulfur (S), and oxygen (O), confirming the successful incorporation of both sulfonic acid groups and iron species. As expected, B-Fe contained the highest Fe content, given that B-TsFe was prepared by mixing equal amounts of B-Ts and B-Fe, and B-Ts lacks iron. These results confirm the successful acid grafting of sulfonic acid groups in B-Ts, iron oxide (Fe^{3+}) in B-Fe, and both functionalities in B-TsFe, as supported by elemental analysis, acid density, and functional group characterization. Furthermore, TEM–EDS mapping (Fig. S7) shows uniform sulfur and iron dispersion in B-TsFe, evidencing an effective Brønsted–Lewis hybrid.

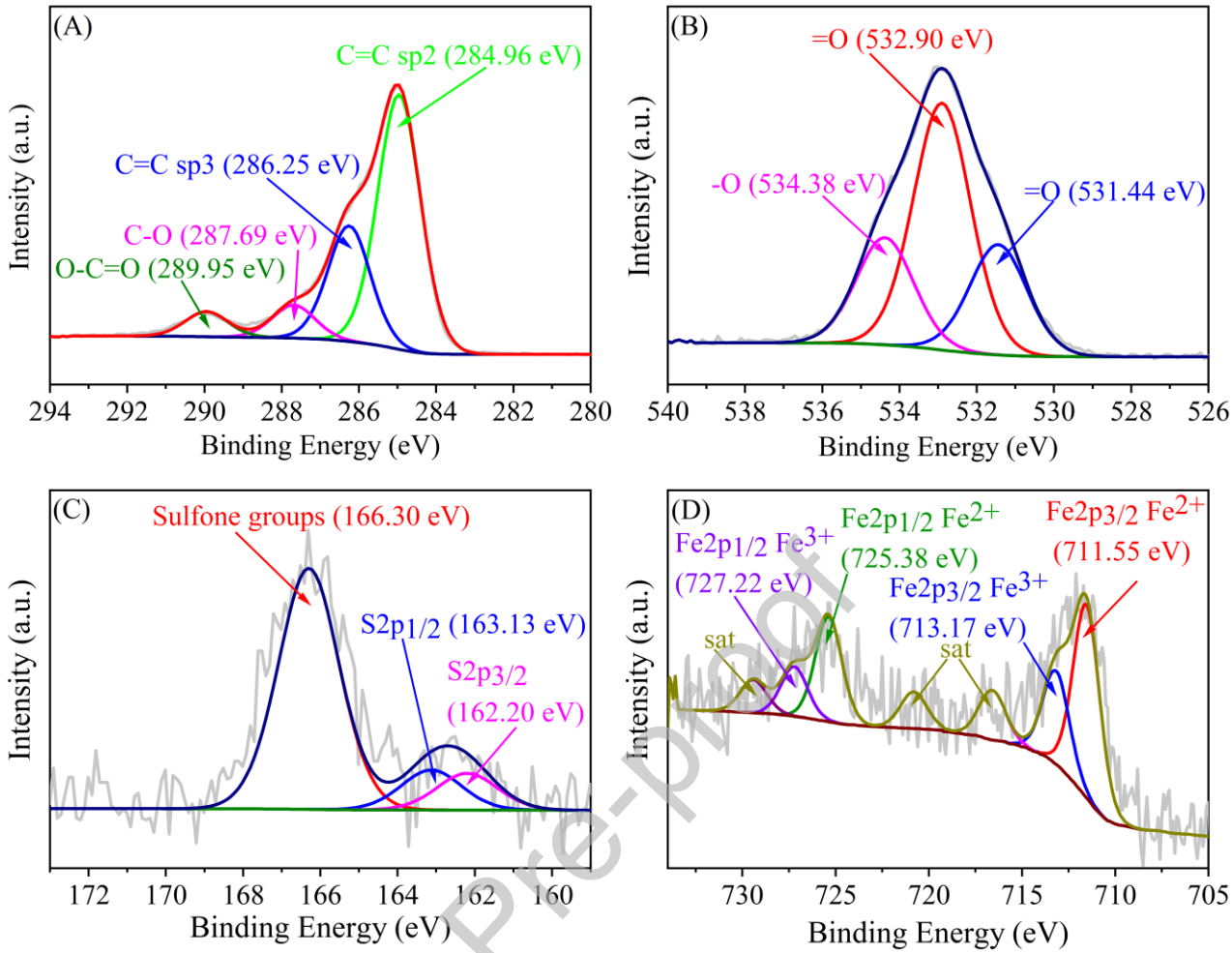

Fig. 4. (A) C1s, (B) O1s, (C) S2p, and (D) Fe2p XPS spectra of B-TsFe catalyst

XPS of B-TsFe (Fig. 4 and Fig. S8) reveals a dominant C 1s peak, indicating the prevalence of carbon–carbon bonds and carbon–oxygen functional groups. Specifically, the C 1s deconvolution showed peaks corresponding to aromatic and aliphatic carbon (C–C/C=C at 284.96 and 286.25 eV) [26, 70], alcohol groups (C-OH, 287.69 eV) [71], and carbonyl functionalities (C=O, 289.95 eV) [72]. The catalyst also exhibited a prominent O 1s signal, confirming the presence of surface oxygenated groups and indicating significant surface oxidation [26]. The O 1s spectrum featured peaks at 531.44 eV and 532.90 eV, corresponding to S=O and C=O bonds in sulfonic and carbonyl groups, respectively [73]. Additionally, the band at 534.38 eV was attributed to single-bonded oxygen atoms from phenolic hydroxyl groups or S–O bonds in sulfonic acid moieties [54, 74, 75]. The S 2p spectrum of the B-TsFe catalyst displayed peaks at 162.20 eV (S $2p_{3/2}$) and 163.13 eV (S $2p_{1/2}$), characteristic of $–SO_3H$

groups, confirming the successful grafting of sulfonic acid functionalities [76]. These strong sulfur and oxygen signals, along with their corresponding binding energies, affirm the incorporation of S=O, S–O, and S–C bonds, highlighting the effective functionalization of the carbon surface derived from CR with covalently bonded –SO_3H groups [77]. Moreover, the high-resolution Fe2p spectrum showed peaks at 711.55 eV and 713.17 eV ($Fe2p_{3/2}$), and 725.38 eV and 727.22 eV ($Fe2p_{1/2}$), consistent with the presence of Fe^{2+} species in iron oxide [78]. These results confirm the successful incorporation of iron species through the $FeCl_3$-assisted grafting process.

3.3. Property of 5-hydroxymethylfurfural in the liquid product

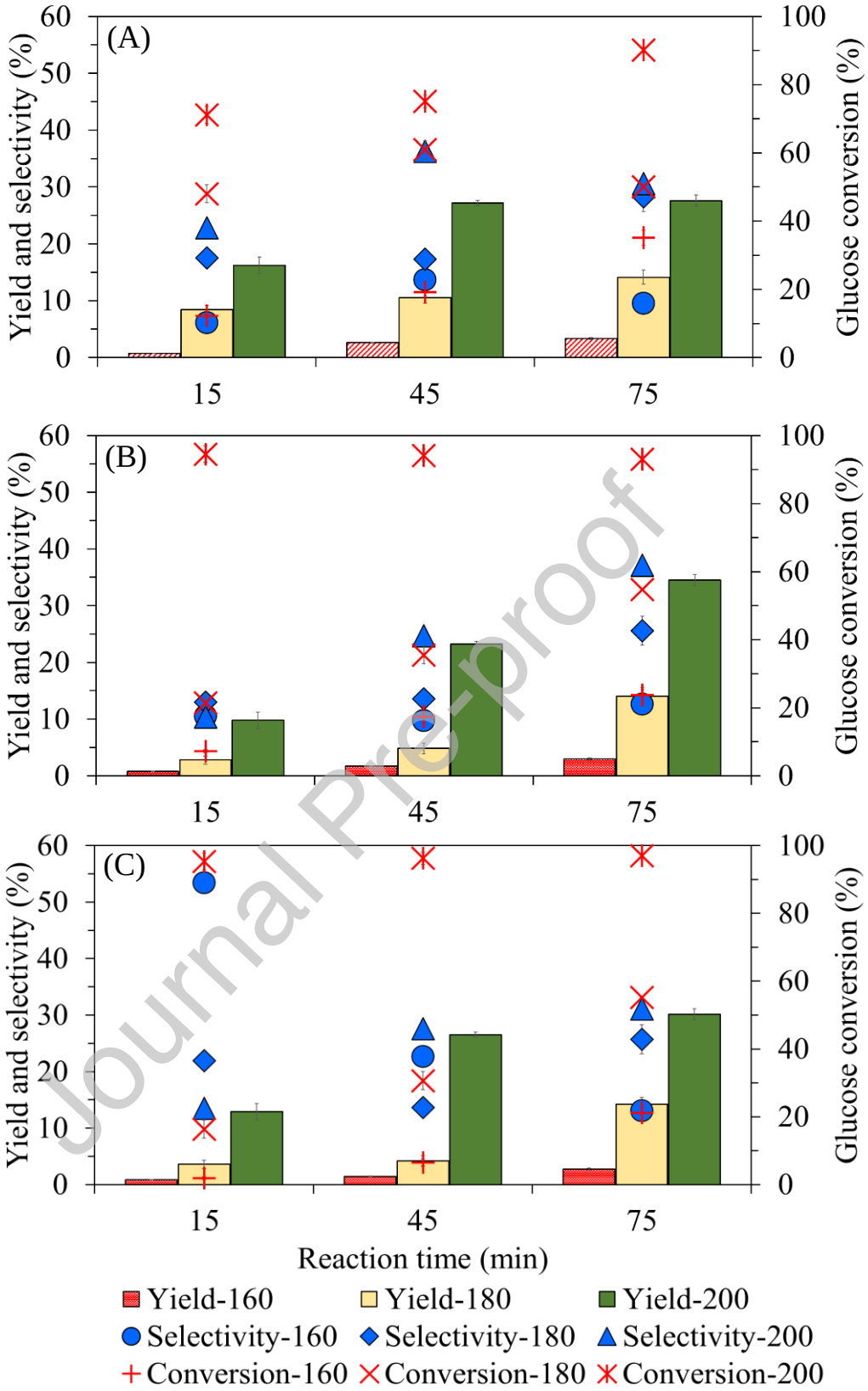

Fig. 5. HMF yield, HMF selectivity, and glucose conversion at 160 – 200°C for 15 – 75 min and iPrOH:H_2O of (A) 4:1, (B) 3:2, and (C) 2:3.

As shown in Table S1, the liquid products obtained from glucose conversion using the CR-derived Brønsted–Lewis hybrid acid catalyst (B-TsFe) in an eco-efficient system primarily consisted of HMF. The influence of key process parameters, including reaction temperature, residence time, and iPrOH:H_2O ratio, on HMF yield, HMF selectivity, and glucose conversion is illustrated in Fig. 5(A)–(F). Temperature and residence time significantly influenced HMF production. At an iPrOH:H_2O ratio of 3:2, increasing the temperature from 160 to 200 °C (at 75 min) and extending the residence time from 15 to 75 min (at 200 °C) improved the HMF yield from 3.0 to 34.5 wt.% and from 9.8 to 34.5 wt.%, respectively. This improvement was primarily due to the isomerization of glucose to fructose, followed by the subsequent triple dehydration of fructose to HMF, as illustrated in Fig. 6 [79]. These trends were consistent with the observed increases in glucose conversion and HMF selectivity. In contrast, varying the iPrOH:H_2O ratio from 4:1 to 2:3 at 200 °C for 75 min resulted in only marginal changes in HMF yield, ranging from 27.6 to 34.5 wt.%. This outcome can be explained by the solvent-dependent solubility and stabilization of both reactants and products [80]. While higher water content enhances the solubility of glucose and fructose, increased iPrOH content favors the solubilization and stabilization of HMF [81]. Thus, the iPrOH:H_2O ratio affects not only solubility but also reaction kinetics, intermediate stabilization, and the balance between isomerization and dehydration reactions, ultimately influencing overall HMF productivity [81, 82]. Under the optimal conditions of 200 °C, 75 min, and iPrOH:H_2O ratio of 3:2, the B-TsFe catalyst achieved a maximum HMF yield of 34.5 wt.% and selectivity of 37.1%.

Among the tested catalysts, B-TsFe yielded the highest HMF production under the optimized conditions (34.5 wt.%), significantly outperforming B-Ts (30.3 wt.%) and B-Fe (26.1 wt.%), as summarized in Table 3. This superior performance is attributed to the synergistic effect of Brønsted and Lewis acid sites on the B-TsFe surface, facilitating both glucose isomerization and fructose dehydration. Compared with other biomass-derived

catalysts, the CR-based B-TsFe catalyst under the iPrOH system (34.5 wt.%) offered a lower HMF yield than the birch sawdust-derived hybrid acid catalyst in a THF system (51.0 wt.%) [26]. This discrepancy is linked to differences in solvent polarity and solvation behavior [83, 84]. THF, with lower polarity and stronger solvation power for organics, improves catalyst–substrate interaction and HMF stability, whereas iPrOH, a moderately polar solvent, offers lower glucose solubility and catalytic efficiency [81, 83]. Nonetheless, iPrOH is considered more sustainable, with a potentially negative carbon footprint, in contrast to THF's positive carbon footprint [85, 86]. Under aqueous conditions, the CR-derived hybrid acid catalyst still outperformed the birch sawdust-derived counterpart. Furthermore, the 34.5 wt.% HMF yield obtained using B-TsFe in the iPrOH system exceeded that achieved with a metallic ZrPO catalyst in a MIBK system (15.6 wt.%) [87]. This advantage stems from the synergistic acidity, strong solvent–catalyst interactions, and favorable solvation characteristics of iPrOH, all of which enhance HMF yield and selectivity while limiting by-product formation. Although ZrPO is catalytically active [88], its performance is hindered in less favorable solvents like MIBK [84], which restrict substrate - catalyst interactions and promote side reactions. In addition, the CR-derived B-TsFe catalyst exhibited superior activity compared to its counterpart derived from cane leaves, which can be attributed to the CR feedstock's lower ash and cellulose contents and higher oxygen, volatile matter, and hemicellulose levels [89]. These compositional features favor porous structure development and acid site functionalization. Overall, the CR-derived B-TsFe catalyst, especially in an iPrOH biphasic system, emerges as a highly promising, sustainable, and effective approach for HMF production from glucose.

Table 3. Comparison of glucose conversion to HMF using biochar-based Brønsted-Lewis hybrid acid catalyst prepared from biomass.

Catalyst synthesis			Reaction conditions			HMF yield (%)
Feedstock	Temperature (°C)	Acid reagent	Temperature (°C)	Time (min)	Solvent media	
CR[This study]	700	TsOH	200	75	iPrOH/H_2O	30.3
CR[This study]	700	$FeCl_3$	200	75	iPrOH/H_2O	26.1
CR[This study]	700	TsOH+$FeCl_3$	200	75	iPrOH/H_2O	34.5
CR[This study]	700	TsOH+$FeCl_3$	160	480	H_2O	26.2
Cane leaf[This study]	700	TsOH+$FeCl_3$	200	75	iPrOH/H_2O	30.2
Tobacco stem [29]	350	TsOH	180	30	GVL/H_2O	43.8
Birch sawdust [26]	800	H_2SO_4+$ZnCl_2$	160	480	H_2O/THF	51.0
Birch sawdust [26]	800	H_2SO_4+$ZnCl_2$	160	480	H_2O	15.0
Peanut shell [58]	-	H_4SO_4	130	120	[Amim]Cl	1.8
Wood residue [90]	700	H_2SO_4+$SnCl_2$	140	240	DMSO	14.8

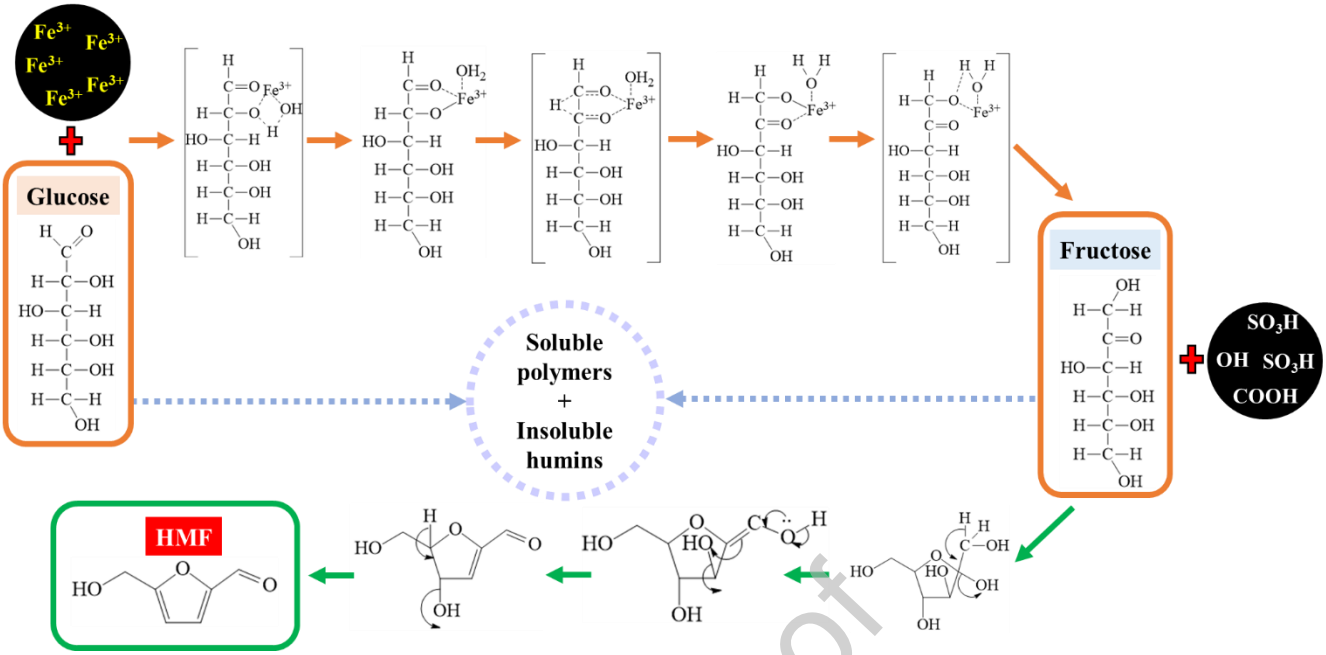

Fig. 6. Proposed reaction mechanisms of glucose conversion to HMF using B-TsFe catalyst [91-93]

3.4. Recycling experiments

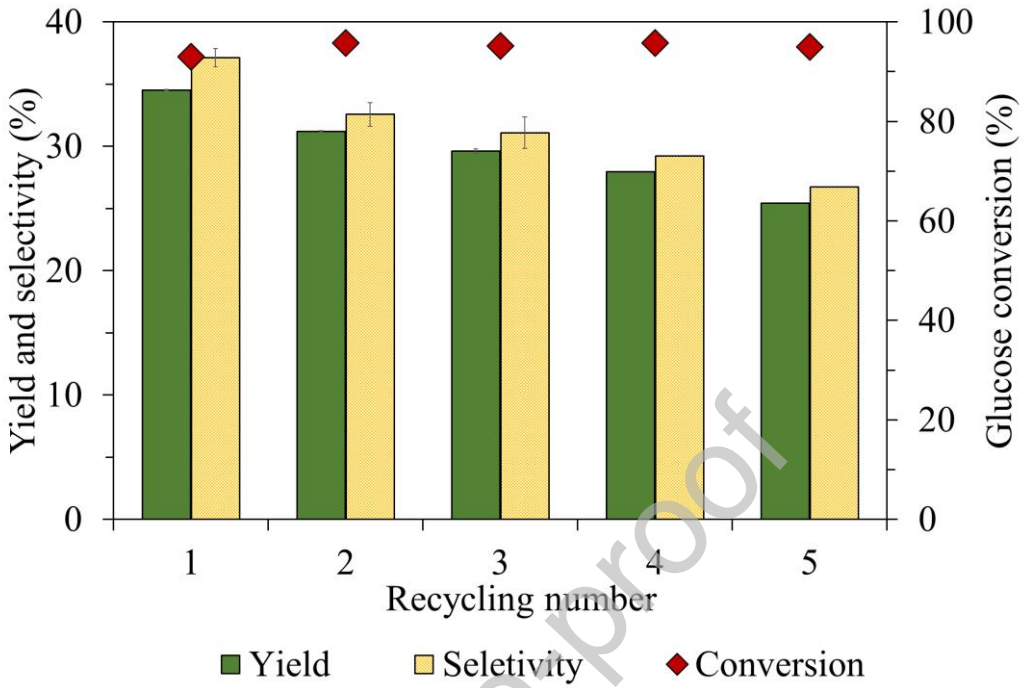

Fig. 7. Effect of B-TsFe catalyst recycling number on HMF yield, HMF selectivity, and glucose conversion

Catalyst reusability is a critical parameter for the commercial viability of HMF synthesis. The stability and reusability of the B-TsFe catalyst, applied at 200 °C for 75 min with an iPrOH:H_2O ratio of 3:2, are illustrated in Fig. 7. After each reaction cycle, the spent catalyst was separated from the liquid product, rinsed with water, and dried at 105 °C for 24 h. The recyclability tests revealed a gradual decline in HMF yield over five consecutive runs, decreasing from 34.5 to 25.4 wt.%, a trend similar to that observed for birch sawdust-derived hybrid acid catalysts [26]. This decline may be attributed to acid site leaching, as well as the accumulation and aggregation of humin or other polymeric by-products on the catalyst surface, mechanistically described in Fig. 6 [94]. These findings are consistent with elemental and surface changes in the spent B-TsFe catalyst, including increased carbon content and reduced

sulfur content, ash content, total acidity, $–SO_3H$ density, and SSA (Table 2). These results emphasize the need for strategies to enhance the long-term durability of CR-based Brønsted–Lewis hybrid acid catalysts. The recyclability of catalysts can be significantly improved through strategies that enhance catalyst stability, mitigate active site leaching (e.g., Fe^{3+} and -SO_3H), and facilitate efficient regeneration processes [26, 95, 96]. The stability of Brønsted and Lewis acid sites can be reinforced through optimized synthesis techniques that ensure robust anchoring of these active groups onto the biochar surface. For instance, employing covalent bonding or introducing stronger anchoring agents to immobilize $–SO_3H$ and Fe^{3+} moieties can effectively minimize leaching during successive catalytic cycles [26]. Moreover, doping or co-doping the biochar matrix with heteroatoms such as nitrogen or sulfur has been shown to enhance both the chemical stability and the longevity of catalytic activity over time [97, 98]. Surface area and porosity, critical parameters influencing catalytic efficiency and reusability, can also be improved via thermal or chemical activation, or through surface functionalization using amines or oxygen-containing groups, thereby facilitating improved glucose adsorption and reaction kinetics in subsequent cycles [96, 99, 100]. Catalyst regeneration is another essential component of maintaining long-term catalytic performance. Effective regeneration can be achieved via thermal treatment in an inert atmosphere to remove carbonaceous fouling and restore active sites [101]; chemical regeneration through acid or base washing to remove surface impurities and reactivate acidic functionalities [102, 103]; and oxidative regeneration or re-impregnation with acidic or functional groups to replenish lost acidity and restore catalytic performance [104]. Implementing these techniques ensures that catalyst activity is sustained across multiple cycles, contributing to a more sustainable and economically viable process for industrial HMF production. Importantly, this study also reconfirms that reaction temperature and residence time are the dominant factors influencing HMF production, while variations in the iPrOH:H_2O ratio exert a comparatively minor effect.

These findings highlight the innovative design and promising efficiency of the B-TsFe catalyst, reinforcing its potential as a high-performance, eco-efficient solution for sustainable HMF production technologies.

4. Conclusion

The efficacy of 5-hydroxymethylfurfural (HMF) production from glucose using a cassava rhizome (CR)-derived biochar-based Brønsted–Lewis hybrid acid catalyst (B-TsFe) was systematically investigated within an eco-efficient solvent system. This study assessed the influence of key operational parameters on HMF yield, including reaction temperature, residence time, and the isopropanol–water (iPrOH:H_2O) solvent ratio. The findings revealed that the B-TsFe catalyst exhibited dual acid functionalities, with both Brønsted and Lewis acid sites confirmed, making it highly effective for promoting glucose conversion. Among the parameters evaluated, reaction temperature and time were found to significantly affect HMF production, while variations in the iPrOH:H_2O ratio had a relatively minor impact. The highest HMF yield of 34.5 wt.% was achieved under optimized conditions (200 °C for 75 min using a 3:2 iPrOH:H_2O ratio). These findings highlight the potential of CR-derived biochar as a sustainable support material for Brønsted–Lewis hybrid acid catalysts in biomass valorization. The approach is applicable to other lignocellulosic feedstocks, though further optimization of functionalization parameters (e.g., sulfonation conditions, Fe loading) may be necessary depending on the precursor's composition (e.g., ash, lignin, cellulose, hemicellulose contents). For broader industrial relevance, future work should include comprehensive life cycle assessment and techno-economic analysis to assess the environmental and economic feasibility of this catalytic strategy.

Declaration of competing interest

The authors declare that they have no known competing financial interests or personal relationships that could have appeared to influence the work reported in this paper.

Data availability

Data will be made available on request.

Acknowledgement

This research project (Grant no. BRF1-069/2565) is supported by Mahidol University (Basic Research Fund: fiscal year 2022). All authors thank Mahidol University Frontier Research Facility (MU-FRF) for instrument support and the MU-FRF scientists, Nawapol Udpuay, Dr. Suwilai Chaveanghong and Bancha Panyacharoen, for their kind assistance in operation of the simultaneous thermogravimetric analyzer and the X-ray diffractometer (XRD).

Declaration of generative AI and AI-assisted technologies in the writing process

During the preparation of this work, the authors used ChatGPT to proofread the English grammar. After using this tool, the authors reviewed and edited the content as needed and took full responsibility for the content of the published article.

References

[1] C. Antonetti, A.M. Raspolli Galletti, S. Fulignati, D. Licursi, Amberlyst A-70: A surprisingly active catalyst for the MW-assisted dehydration of fructose and inulin to HMF in water, Catal. Commun. 97 (2017) 146-150.

[2] A. Gandini, M.N. Belgacem, Recent contributions to the preparation of polymers derived from renewable resources, J. Polym. Environ. 10 (2002) 105-114.

[3] Z. Huang, X. Sun, W. Zhao, X. Zhu, Z. Zeng, Q. Xu, X. Liu, Selective hydroconversion of 5-hydroxymethylfurfural to 2,5-bis(hydroxymethyl)furan using carbon nanotubes-supported nickel catalysts, Carbon Resour. Convers. 5 (2022) 289-298.

[4] W. Zhao, F. Wang, K. Zhao, X. Liu, X. Zhu, L. Yan, Y. Yin, Q. Xu, D. Yin, Recent advances in the catalytic production of bio-based diol 2,5-bis(hydroxymethyl)furan, Carbon Resour. Convers. 6 (2023) 116-131.

[5] X. Liao, H. Cui, H. Luo, Y. Lv, P. Liu, Highly efficient selective hydrodeoxygenation of 5-hydroxymethylfurfural to 2,5-dimethylfuran over Co-Ni in-situ encapsulated in biochar-based carbon catalysts: The crucial role of CoNi alloys and Co-Nx species, Chem. Eng. J. 503 (2025) 158336.

[6] Y. Cui, Z. Yang, X. Hu, S. Yang, A. Rezayan, T. Lu, Z. Chen, Y. Zhang, Highly efficient isomerization of glucose to fructose over Sn-doped silica nanotube, Resour. Chem. Mater. 3 (2024) 159-165.

[7] J. Wang, W. Xu, J. Ren, X. Liu, G. Lu, Y. Wang, Efficient catalytic conversion of fructose into hydroxymethylfurfural by a novel carbon-based solid acid, Green Chem. 13 (2011) 2678-2681.

[8] P. Daorattanachai, P. Khemthong, N. Viriya-empikul, N. Laosiripojana, K. Faungnawakij, Conversion of fructose, glucose, and cellulose to 5-hydroxymethylfurfural by alkaline earth phosphate catalysts in hot compressed water, Carbohydr. Res. 363 (2012) 58-61.

[9] P. Khemthong, C. Yimsukanan, T. Narkkun, A. Srifa, T. Witoon, S. Pongchaiphol, S. Kiatphuengporn, K. Faungnawakij, Advances in catalytic production of value-added biochemicals and biofuels via furfural platform derived lignocellulosic biomass, Biomass Bioenergy. 148 (2021) 106033.

[10] P. Khemthong, P. Daorattanachai, N. Laosiripojana, K. Faungnawakij, Copper phosphate nanostructures catalyze dehydration of fructose to 5-hydroxymethylfufural, Catal. Commun. 29 (2012) 96-100.

[11] G. Phachwisoot, K. Nakason, C. Chanthad, P. Khemthong, W. Kraithong, S. Youngjan, B. Panyapinyopol, Sequential Production of Levulinic Acid and Supercapacitor Electrode Materials from Cassava Rhizome through an Integrated Biorefinery Process, ACS Sustain. Chem. Eng. 9 (2021) 7824-7836.

[12] T.K. Godan, L.P. Devendra, M.P. Alphy, R.O. Rajesh, N. Vivek, R. Sindhu, M.K. Awasthi, P. Binod, Catalytic synthesis of 5-hydroxymethyl furfural from sorghum syrup derived fructose, Sustain. Energy Technol. Assess. 54 (2022) 102884.

[13] F. Shahangi, A. Najafi Chermahini, M. Saraji, Dehydration of fructose and glucose to 5-hydroxymethylfurfural over Al-KCC-1 silica, J. Energy Chem. 27 (2018) 769-780.

[14] S. Zhou, W. Liu, D. Liu, X. Shi, K. Huang, F. Jiang, H. Gao, H. Xia, Y. Guan, S. Xu, Promoting 5-hydroxymethylfurfural production from cellulose and wheat straw via sulfonic acid group-grafted SBA-15 mesoporous silica embedded with iron phosphate, Ind. Crop. Prod. 233 (2025) 121425.

[15] S. Marullo, C. Rizzo, A. Meli, F. D'Anna, Ionic Liquid Binary Mixtures, Zeolites, and Ultrasound Irradiation: A Combination to Promote Carbohydrate Conversion into 5-Hydroxymethylfurfural, ACS Sustain. Chem. Eng. 7 (2019) 5818-5826.

[16] M. Besson, P. Gallezot, C. Pinel, Conversion of Biomass into Chemicals over Metal Catalysts, Chem. Rev. 114 (2014) 1827-1870.

[17] C. Tempelman, U. Jacobs, T. Hut, E. Pereira de Pina, M. van Munster, N. Cherkasov, V. Degirmenci, Sn exchanged acidic ion exchange resin for the stable and continuous production of 5-HMF from glucose at low temperature, Appl. Catal. A Gen. 588 (2019) 117267.

[18] K. Nakason, P. Sumrannit, S. Youngjan, W. Wanmolee, W. Kraithong, P. Khemthong, V. Kanokkantapong, B. Panyapinyopol, Environmental impact of 5-hydroxymethylfurfural production from cellulosic sugars using biochar-based acid catalyst, Chem. Eng. Sci. 287 (2024) 119729.

[19] K. AL-TWAL, Carbon Footprint Assessment Of Biochar Production From Biomass Via Pyrolysis, Department Of Civil, Environmental and Architectural Engineering, UNIVERSITÀ DEGLI STUDI DI PADOVA. https://thesis.unipd.it/retrieve/fb90608b-2876-4715-9a96-7ea8b67f7e19/Al-Twal_KareemOsamaFakhri%20.pdf, 2023 (accessed 30 May 2025).

[20] K.N. Shoudho, T.H. Khan, U.R. Ara, M.R. Khan, Z.B.Z. Shawon, M.E. Hoque, Biochar in global carbon cycle: Towards sustainable development goals, Curr. Res. Green Sustain. 8 (2024) 100409.

[21] L.J. Snowden-Swan, K.A. Spies, G.J. Lee, Y. Zhu, Life cycle greenhouse gas emissions analysis of catalysts for hydrotreating of fast pyrolysis bio-oil, Biomass Bioenergy. 86 (2016) 136-145.

[22] S. Bustillos, M. Christofides, B. McDevitt, M. Blondes, R. McAleer, A.M. Jubb, B. Wang, G. Sant, D. Simonetti, Ion Exchange Processes for CO2 Mineralization Using Industrial Waste Streams: Pilot Plant Demonstration and Life Cycle Assessment, ChemistrySelect. 9 (2024) e202400834.

[23] A.-N. Parvulescu, S. Maurer, Toward sustainability in zeolite manufacturing: An industry perspective, Front. Chem. Volume 10 - 2022 (2022).

[24] H.U. Escobar-Hernandez, Y. Quan, M.I. Papadaki, Q. Wang, Life Cycle Assessment of Metal–Organic Frameworks: Sustainability Study of Zeolitic Imidazolate Framework-67, ACS Sustain. Chem. Eng. 11 (2023) 4219-4225.

[25] A. Kuntinuguntanon, S. Roddecha, S. Pumrod, A. Jaree, A. Kaewchada, The Implementation of Dual Lewis and BrØnsted Acidic Functionalized Carbon Supported Solid Acid Catalysts Derived from Palm Oil Empty Fruit Bunch for 5-Hydroxy Methylfurfural (5-HMF) Production, Waste Biomass Valorization. 13 (2022) 383-403.

[26] A. Rusanen, R. Lahti, K. Lappalainen, J. Kärkkäinen, T. Hu, H. Romar, U. Lassi, Catalytic conversion of glucose to 5-hydroxymethylfurfural over biomass-based activated carbon catalyst, Catal. Today. 357 (2020) 94-101.

[27] H. Guo, X. Ma, Z. Chen, J. Guo, J. Lu, Efficient 5-hydroxymethylfurfural production in ChCl-based deep eutectic solvents using boric acid and metal chlorides, RSC Adv. 15 (2025) 3664-3671.

[28] K. Nakason, P. Khemthong, W. Kraithong, P. Chukaew, B. Panyapinyopol, D. Kitkaew, P. Pavasant, Upgrading properties of biochar fuel derived from cassava rhizome via torrefaction: Effect of sweeping gas atmospheres and its economic feasibility, Case Stud. Therm. Eng. 23 (2021) 100823.

[29] F. Huang, W. Li, Q. Liu, T. Zhang, S. An, D. Li, X. Zhu, Sulfonated tobacco stem carbon as efficient catalyst for dehydration of C6 carbohydrate to 5-hydroxymethylfurfural in γ-valerolactone/water, Fuel Process. Technol. 181 (2018) 294-303.

[30] S.P. Teong, G. Yi, Y. Zhang, Hydroxymethylfurfural production from bioresources: past, present and future, Green Chem. 16 (2014) 2015-2026.

[31] H. Wang, Q. Kong, Y. Wang, T. Deng, C. Chen, X. Hou, Y. Zhu, Graphene Oxide Catalyzed Dehydration of Fructose into 5-Hydroxymethylfurfural with Isopropanol as Cosolvent, ChemCatChem. 6 (2014) 728-732.

[32] L. Lai, Y. Zhang, The Production of 5-Hydroxymethylfurfural from Fructose in Isopropyl Alcohol: A Green and Efficient System, ChemSusChem. 4 (2011) 1745-1748.

[33] K. Inokuma, J.C. Liao, M. Okamoto, T. Hanai, Improvement of isopropanol production by metabolically engineered Escherichia coli using gas stripping, J. Biosci. Bioeng. 110 (2010) 696-701.

[34] P. Chukaew, K. Nakason, S. Kuboon, W. Kraithong, B. Panyapinyopol, K. Vorapot, Conversion of cassava rhizome to biocrude oil via hydrothermal liquefaction, Int. Energy J. 21 (2021) 269 - 280.

[35] K. Nakason, B. Panyapinyopol, V. Kanokkantapong, N. Viriya-empikul, W. Kraithong, P. Pavasant, Characteristics of hydrochar and liquid fraction from hydrothermal carbonization of cassava rhizome, J. Energy Inst. 91 (2018) 184-193.

[36] Sluiter, A., Hames, B., Ruiz, R., Scarlata, C., Sluiter, J., Templeton, D. (2008) Determination of ash in biomass (NREL/TP-510-42622). The US national renewable energy laboratory technical report.

[37] T. Liu, Z. Li, W. Li, C. Shi, Y. Wang, Preparation and characterization of biomass carbon-based solid acid catalyst for the esterification of oleic acid with methanol, Bioresour. Technol. 133 (2013) 618-621.

[38] Y. Hu, M. Li, Z. Gao, L. Wang, J. Zhang, Leaf-derived sulfonated carbon dots: efficient and recoverable catalysts to synthesize 5-hydroxymethylfurfural from fructose, Mater. Today Chem. 20 (2021) 100423.

[39] A. Sluiter, B. Hames, R. Ruiz, C. Scarlata, J. Sluiter, D. Templeton, D. Crocker. Determination of structural carbohydrates and lignin in biomass (NREL/TP510-42618). The US National Renewable Energy Laboratory technical report.

[40] ASTM. 2010. Standard Test Methods for Proximate Analysis of Coal and Coke by Macro Thermogravimetric Analysis. Method D7582-10. ASTM International, Pennsylvania.

[41] L.-P. Xiao, Z.-J. Shi, F. Xu, R.-C. Sun, Hydrothermal carbonization of lignocellulosic biomass, Bioresour. Technol. 118 (2012) 619-623.

[42] X. Yuan, Y. Cao, J. Li, A.K. Patel, C.-D. Dong, X. Jin, C. Gu, A.C.K. Yip, D.C.W. Tsang, Y.S. Ok, Recent advancements and challenges in emerging applications of biochar-based catalysts, Biotechnol. Adv. 67 (2023) 108181.

[43] R. Shu, H. Jiang, L. Xie, X. Liu, T. Yin, Z. Tian, C. Wang, Y. Chen, Efficient hydrodeoxygenation of lignin-derived phenolic compounds by using Ru-based biochar catalyst coupled with silicotungstic acid, Renew. Energy. 202 (2023) 1160-1168.

[44] Z.D. Hood, Y. Cheng, S.F. Evans, S.P. Adhikari, M. Parans Paranthaman, Unraveling the structural properties and dynamics of sulfonated solid acid carbon catalysts with neutron vibrational spectroscopy, Catal. Today 358 (2020) 387-393.

[45] Fitria, J. Liu, B. Yang, Roles of mineral matter in biomass processing to biofuels, Biofuels Bioprod. Biorefining. 17 (2023) 696-717.

[46] C. Wang, Q. He, W. Chen, Q. Cheng, G. Song, G. Fan, Synthesis of 5-hydroxymethylfurfural from glucose over carbon-based acid–base bifunctional catalyst, Energy sci. eng. 11 (2023) 2408-2420.

[47] S. Liu, Y. Zhu, Y. Liao, H. Wang, Q. Liu, L. Ma, C. Wang, Advances in understanding the humins: Formation , prevention and application, Appl. Energy Combust. Sci. 10 (2022) 100062.

[48] H.S. Kulkarni, P.A. Kamble, C.P. Vinod, V.K. Rathod, M.L. Kantam, Synthesis of 5-hydroxymethylfurfural from glucose using a tert-butoxyapatite catalyst, Dalton Trans. 54 (2025) 13574-13587.

[49] P. Wataniyakul, P. Boonnoun, A.T. Quitain, M. Sasaki, T. Kida, N. Laosiripojana, A. Shotipruk, Preparation of hydrothermal carbon as catalyst support for conversion of biomass to 5-hydroxymethylfurfural, Catal. Commun. 104 (2018) 41-47.

[50] S. Chellappan, V. Nair, S. V, A. K, Experimental validation of biochar based green Bronsted acid catalysts for simultaneous esterification and transesterification in biodiesel production, Bioresour. Technol. Rep. 2 (2018) 38-44.

[51] J. Wang, J. Ren, X. Liu, G. Lu, Y. Wang, High yield production and purification of 5-hydroxymethylfurfural, AIChE J. 59 (2013) 2558-2566.

[52] M.S.A. Farabi, M.L. Ibrahim, U. Rashid, Y.H. Taufiq-Yap, Esterification of palm fatty acid distillate using sulfonated carbon-based catalyst derived from palm kernel shell and bamboo, Energy Convers. Manag. 181 (2019) 562-570.

[53] F. Lónyi, J. Valyon, On the interpretation of the NH3-TPD patterns of H-ZSM-5 and H-mordenite, Microporous Mesoporous Mater. 47 (2001) 293-301.

[54] P.P. Upare, J.-W. Yoon, M.Y. Kim, H.-Y. Kang, D.W. Hwang, Y.K. Hwang, H.H. Kung, J.-S. Chang, Chemical conversion of biomass-derived hexose sugars to levulinic acid over sulfonic acid-functionalized graphene oxide catalysts, Green Chem. 15 (2013) 2935-2943.

[55] S. Kang, J. Ye, Y. Zhang, J. Chang, Preparation of biomass hydrochar derived sulfonated catalysts and their catalytic effects for 5-hydroxymethylfurfural production, RSC Adv. 3 (2013) 7360-7366.

[56] H.T. Gomes, S.M. Miranda, M.J. Sampaio, J.L. Figueiredo, A.M.T. Silva, J.L. Faria, The role of activated carbons functionalized with thiol and sulfonic acid groups in catalytic wet peroxide oxidation, Appl. Catal. B: Environ. 106 (2011) 390-397.

[57] X. Xiong, I.K.M. Yu, S.S. Chen, D.C.W. Tsang, L. Cao, H. Song, E.E. Kwon, Y.S. Ok, S. Zhang, C.S. Poon, Sulfonated biochar as acid catalyst for sugar hydrolysis and dehydration, Catal. Today. 314 (2018) 52-61.

[58] K.-L. Chang, S.C. Muega, B.I.G. Ofrasio, W.-H. Chen, E.G. Barte, R.R.M. Abarca, M.D.G. de Luna, Synthesis of 5-hydroxymethylfurfural from glucose, fructose, cellulose

and agricultural wastes over sulfur-doped peanut shell catalysts in ionic liquid, Chemosphere. 291 (2022) 132829.

[59] L. Liu, X. Yang, Q. Hou, S. Zhang, M. Ju, Corn stalk conversion into 5-hydroxymethylfurfural by modified biochar catalysis in a multi-functional solvent, J. Clean. Prod. 187 (2018) 380-389.

[60] J. Zhao, C. Zhou, C. He, Y. Dai, X. Jia, Y. Yang, Efficient dehydration of fructose to 5-hydroxymethylfurfural over sulfonated carbon sphere solid acid catalysts, Catal. Today. 264 (2016) 123-130.

[61] J. Yang, H. Zhang, Z. Ao, S. Zhang, Hydrothermal carbon enriched with sulfonic and carboxyl groups as an efficient solid acid catalyst for butanolysis of furfuryl alcohol, Catal. Commun., 123 (2019) 109-113.

[62] A.P. da Luz Corrêa, R.R.C. Bastos, G.N.d. Rocha Filho, J.R. Zamian, L.R.V.d. Conceição, Preparation of sulfonated carbon-based catalysts from murumuru kernel shell and their performance in the esterification reaction, RSC Adv. 10 (2020) 20245-20256.

[63] H. Shirai, S. Ikeda, E.W. Qian, One-pot production of 5-hydroxymethylfurfural from cellulose using solid acid catalysts, Fuel Process. Technol. 159 (2017) 280-286.

[64] M. Gopiraman, D. Deng, B.-S. Kim, I.-M. Chung, I.S. Kim, Three-dimensional cheese-like carbon nanoarchitecture with tremendous surface area and pore construction derived from corn as superior electrode materials for supercapacitors, Appl. Surf. Sci. 409 (2017) 52-59.

[65] Y. Fan, P.-F. Liu, Z.-J. Yang, T.-W. Jiang, K.-L. Yao, R. Han, X.-X. Huo, Y.-Y. Xiong, Bi-functional porous carbon spheres derived from pectin as electrode material for supercapacitors and support material for Pt nanowires towards electrocatalytic methanol and ethanol oxidation, Electrochim. Acta. 163 (2015) 140-148.

[66] J.-B. Wu, M.-L. Lin, X. Cong, H.-N. Liu, P.-H. Tan, Raman spectroscopy of graphene-based materials and its applications in related devices, Chem. Soc. Rev. 47 (2018) 1822-1873.

[67] N. Shimodaira, A. Masui, Raman spectroscopic investigations of activated carbon materials, J. Appl. Phys. 92 (2002) 902-909.

[68] C. Lokmit, K. Nakason, S. Kuboon, A. Jiratanachotikul, B. Panyapinyopol, A comparison of char fuel properties derived from dry and wet torrefaction of oil palm leaf and its techno-economic feasibility, Mater. Sci. Energy Technol. 6 (2023) 192-204.

[69] M.A.A.B.A. Rani, N.A. Karim, S.K. Kamarudin, Microporous and mesoporous structure catalysts for the production of 5-hydroxymethylfurfural (5-HMF), Int. J. Energy Res. 46 (2022) 577-633.

[70] Y. Zhong, P. Zhang, X. Zhu, H. Li, Q. Deng, J. Wang, Z. Zeng, J.-J. Zou, S. Deng, Highly Efficient Alkylation Using Hydrophobic Sulfonic Acid-Functionalized Biochar as a Catalyst for Synthesis of High-Density Biofuels, ACS Sustain. Chem. Eng. 7 (2019) 14973-14981.

[71] R.E.C. Torrejos, E.C. Escobar, J.W. Han, S.H. Min, H. Yook, K.J. Parohinog, S. Koo, H. Kim, G.M. Nisola, W.-J. Chung, Multidentate thia-crown ethers as hyper-crosslinked macroporous adsorbent resins for the efficient Pd/Pt recovery and separation from highly acidic spent automotive catalyst leachate, Chem. Eng. J. 424 (2021) 130379.

[72] Q. Li, M. Hu, K. Wang, X. Wang, One-step approach for fabrication of 3D porous carbon/graphene composites as supercapacitor electrode materials, Catal. Today. 330 (2019) 228-239.

[73] A.P. da Luz Corrêa, P.M.M. da Silva, M.A. Gonçalves, R.R.C. Bastos, G.N. da Rocha Filho, L.R.V. da Conceição, Study of the activity and stability of sulfonated carbon

catalyst from agroindustrial waste in biodiesel production: Influence of pyrolysis temperature on functionalization, Arab. J. Chem. 16 (2023) 104964.

[74] P. Rechnia-Gorący, A. Malaika, M. Kozłowski, Acidic activated carbons as catalysts of biodiesel formation, Diam. Relat. Mater. 87 (2018) 124-133.

[75] P. Burg, P. Fydrych, D. Cagniant, G. Nanse, J. Bimer, A. Jankowska, The characterization of nitrogen-enriched activated carbons by IR, XPS and LSER methods, Carbon. 40 (2002) 1521-1531.

[76] Q. Shu, J. Gao, Z. Nawaz, Y. Liao, D. Wang, J. Wang, Synthesis of biodiesel from waste vegetable oil with large amounts of free fatty acids using a carbon-based solid acid catalyst, Appl. Energy. 87 (2010) 2589-2596.

[77] P.M. Ganje, S.A. Jabasingh, S.K. Kassahun, H. Kim, Sulfonated graphitic carbon catalyst derived from coffee waste: A sustainable valorization approach for highly efficient production of 5-hydroxymethylfurfural (5-HMF) from fructose, J. Environ. Chem. Eng. 12 (2024) 113639.

[78] L. Li, P. Ma, S. Hussain, L. Jia, D. Lin, X. Yin, Y. Lin, Z. Cheng, L. Wang, FeS2/carbon hybrids on carbon cloth: a highly efficient and stable counter electrode for dye-sensitized solar cells, Sustain. Energy Fuels. 3 (2019) 1749-1756.

[79] H. An, Y.W. Kim, S. Kweon, Y.M. Son, J.F. Kim, C.-H. Shin, S.B. Kang, M.B. Park, H.-K. Min, Cascade conversion of glucose to 5-hydroxymethylfurfural over Brønsted–Lewis bi-acidic SiO2–ZrO2 catalysts, Biomass Convers. Biorefinery. 13 (2023) 11779-11787.

[80] I.K.M. Yu, D.C.W. Tsang, Conversion of biomass to hydroxymethylfurfural: A review of catalytic systems and underlying mechanisms, Bioresour. Technol. 238 (2017) 716-732.

[81] H. Li, Z. Xia, P. Yan, Z.C. Zhang, Production of crude 5-hydroxymethylfurfural from glucose by dual catalysts with functional promoters in low-boiling hybrid solvent, Catal. Today. (2022).

[82] M. Nahavandi, T. Kasanneni, Z.S. Yuan, C.C. Xu, S. Rohani, Efficient Conversion of Glucose into 5-Hydroxymethylfurfural Using a Sulfonated Carbon-Based Solid Acid Catalyst: An Experimental and Numerical Study, ACS Sustain. Chem. Eng. 7 (2019) 11970-11984.

[83] M.-C. Shih, L.-K. Chu, Does Tetrahydrofuran (THF) Behave like a Solvent or a Reactant in the Photolysis of Thionyl Chloride (Cl2SO) in Cyclohexane? A Transient Infrared Difference Study, J. Phys. Chem. A. 122 (2018) 5401-5408.

[84] J. Liang, J. Jiang, T. Cai, C. Liu, J. Ye, X. Zeng, K. Wang, Advances in selective conversion of carbohydrates into 5-hydroxymethylfurfural, Green Energy Environ. 9 (2024) 1384-1406.

[85] C.S. Slater, S.M. J., H. David, E.J. and Cavanagh, Environmental analysis of the life cycle emissions of 2-methyl tetrahydrofuran solvent manufactured from renewable resources, J. Environ. Sci. Health - Toxic/Hazard. Subst. Environ. Eng. 51 (2016) 487-494.

[86] F.E. Liew, R. Nogle, T. Abdalla, B.J. Rasor, C. Canter, R.O. Jensen, L. Wang, J. Strutz, P. Chirania, S. De Tissera, A.P. Mueller, Z. Ruan, A. Gao, L. Tran, N.L. Engle, J.C. Bromley, J. Daniell, R. Conrado, T.J. Tschaplinski, R.J. Giannone, R.L. Hettich, A.S. Karim, S.D. Simpson, S.D. Brown, C. Leang, M.C. Jewett, M. Köpke, Carbon-negative production of acetone and isopropanol by gas fermentation at industrial pilot scale, Nat. Biotechnol. 40 (2022) 335-344.

[87] V.V. Ordomsky, V.L. Sushkevich, J.C. Schouten, J. van der Schaaf, T.A. Nijhuis, Glucose dehydration to 5-hydroxymethylfurfural over phosphate catalysts, J. Catal. 300 (2013) 37-46.

[88] K.H.P. Reddy, J. Lee, Y.-K. Park, Hydroxymethylfurfural production from cellulosic sugars over supported metal and metal oxide catalysts, Ind. Crops Prod. 222 (2024) 119754.

[89] K. Nakason, P. Chukaew, F. Utrarachkij, S. Kuboon, W. Kraithong, S. Pichaiyut, W. Wanmolee, B. Panyapinyopol, Antimicrobial and antioxidant activities of lignin by-product from sugarcane leaf conversion to levulinic acid and hydrochar, Sustain. Mater. Technol. 40 (2024) e00973.

[90] M. Zuo, Q. Niu, Y. Zhu, S. Li, W. Jia, Z. Zhou, X. Zeng, L. Lin, Biochar catalysts for efficiently 5-Hydroxymethylfurfural (HMF) synthesis in aqueous natural deep eutectic solvent (A-NADES), Ind. Crops Prod. 192 (2023) 115953.

[91] V. Choudhary, S.H. Mushrif, C. Ho, A. Anderko, V. Nikolakis, N.S. Marinkovic, A.I. Frenkel, S.I. Sandler, D.G. Vlachos, Insights into the Interplay of Lewis and Brønsted Acid Catalysts in Glucose and Fructose Conversion to 5-(Hydroxymethyl)furfural and Levulinic Acid in Aqueous Media, J. Am. Chem. Soc., 135 (2013) 3997-4006.

[92] P. Bhaumik, P.L. and Dhepe, Solid acid catalyzed synthesis of furans from carbohydrates, Catal. Rev. 58 (2016) 36-112.

[93] D. Steinbach, A. Klier, A. Kruse, J. Sauer, S. Wild, M. Zanker, Isomerization of Glucose to Fructose in Hydrolysates from Lignocellulosic Biomass Using Hydrotalcite, Processes. 2020.

[94] A. Deng, Q. Lin, Y. Yan, H. Li, J. Ren, C. Liu, R. Sun, A feasible process for furfural production from the pre-hydrolysis liquor of corncob via biochar catalysts in a new biphasic system, Bioresour. Technol. 216 (2016) 754-760.

[95] R. Foroutan, R. Mohammadi, J. Razeghi, B. Ramavandi, Biodiesel production from edible oils using algal biochar/CaO/K2CO3 as a heterogeneous and recyclable catalyst, Renew. Energy. 168 (2021) 1207-1216.

[96] F. Cheng, X. Li, Preparation and Application of Biochar-Based Catalysts for Biofuel Production, Catalysts. 2018.

[97] K. Morawa Eblagon, R.G. Morais, A. Malaika, M.A. Castro Bravo, N. Rey-Raap, M.F.R. Pereira, M. Kozłowski, Production of 5-Hydroxymethylfurfural (HMF) from Sucrose in Aqueous Phase Using S, N-Doped Hydrochars, Catalysts. 2025.

[98] H. Zhang, J.H. Clark, T. Geng, H. Zhang, F. Cao, A Carbon Catalyst Co-Doped with P and N for Efficient and Selective Oxidation of 5-Hydroxymethylfurfural into 2,5-Diformylfuran, ChemSusChem. 14 (2021) 456-466.

[99] C. Zhao, Q. Xu, Y. Gu, X. Nie, R. Shan, Review of Advances in the Utilization of Biochar-Derived Catalysts for Biodiesel Production, ACS Omega. 8 (2023) 8190-8200.

[100] E.T.C. Vogt, D. Fu, B.M. Weckhuysen, Carbon Deposit Analysis in Catalyst Deactivation, Regeneration, and Rejuvenation, Angew. Chem. Int. Ed. 62 (2023) e202300319.

[101] M.M. Nkiawete, R.V. Wal, Thermo-Catalytic Decomposition Comparisons: Carbon Catalyst Structure, Hydrocarbon Feed and Regeneration, Catalysts. 2023.

[102] V. Daligaux, R. Richard, M.-H. Manero, Deactivation and Regeneration of Zeolite Catalysts Used in Pyrolysis of Plastic Wastes—A Process and Analytical Review, Catalysts. 2021.

[103] M. Sheintuch, Y.I. Matatov-Meytal, Comparison of catalytic processes with other regeneration methods of activated carbon, Catal. Today. 53 (1999) 73-80.

[104] J. Zhou, J. Zhao, J. Zhang, T. Zhang, M. Ye, Z. Liu, Regeneration of catalysts deactivated by coke deposition: A review, Chin J Catal. 41 (2020) 1048-1061.

Graphical Abstract

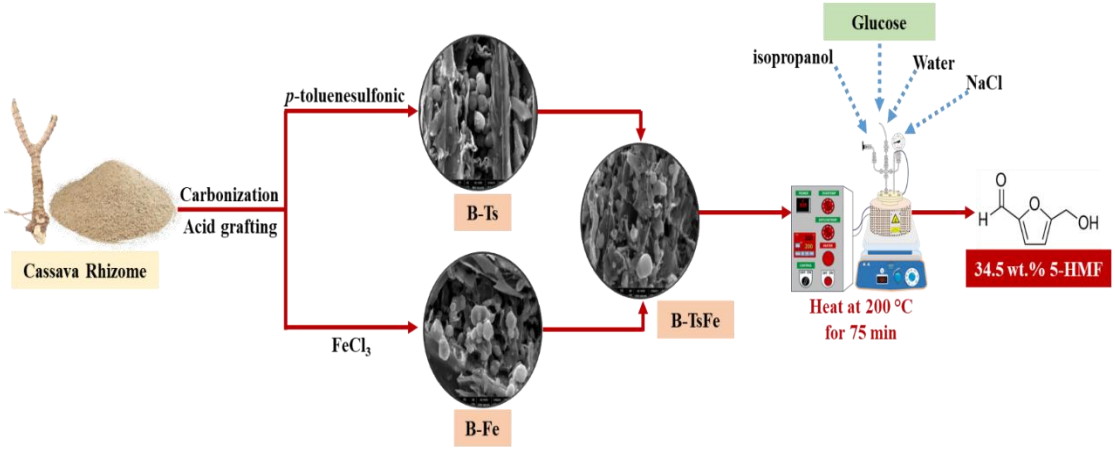

Declaration of interests

☒ The authors declare that they have no known competing financial interests or personal relationships that could have appeared to influence the work reported in this paper.